Electronic Supplementary Material (ESI) for Materials Horizons.

Supporting Information

An Unsymmetrical Thermally Activated Delayed Fluorescence Emitter Enables Orange-Red Electroluminescence with 31.7% External Quantum Efficiency

Xuan Zeng,†[ab] Yu-Hsin Huang,†[c] Shaolong Gong,*[ad] Pan Li,[c] Wei-Kai Lee,[c] Xiao Xiao,[a] Yu Zhang,[a] Cheng Zhong,[a] Chung-Chih Wu*[c] and Chuluo Yang*[ab]

[a]Department of Chemistry, Renmin Hospital of Wuhan University, Hubei Key Lab on Organic and Polymeric Optoelectronic Materials, Wuhan University, Wuhan, 430072, P. R. China. E-mail: slgong@whu.edu.cn; clyang@whu.edu.cn

[b]College of Materials Science and Engineering, Shenzhen University, Shenzhen 518060, People's Republic of China.

[c]Department of Electrical Engineering, Graduate Institute of Electronics Engineering, and Graduate Institute of Photonics and Optoelectronics, National Taiwan University, Taipei 10617, Taiwan. E-mail: wucc@ntu.edu.tw

[d]Shenzhen Research Institute of Wuhan University, Shenzhen 518057, People's Republic of China

†X. Zeng and Y.-H. Huang contributed equally to this work

Table of Contents

Experimental Procedures

General Information

Toluene was dried by sodium-potassium alloy. 9,9'(10*H*,10'*H*)-spirobiacridines, 6-bromo-2-phenyl-1*H*-benzo[*de*]isoquinoline-1,3(2*H*)-dione, 10-(4-(4,6-diphenyl-1,3,5-triazin-2-yl)phenyl)-9,9-dimethyl-9,10-dihydroacridine (DMAC-TRZ) and 6-(9,9-dimethylacridin-10(9*H*)-yl)-2-phenyl-1*H*-benzo[*de*]isoquinoline-1,3(2*H*)-dione (6AcBIQ) were synthesized according to previous reports.[1] The other reagents and solvents were used as received from commercial sources without further purification. ^{1}H NMR and ^{13}C NMR spectra were recorded by Bruker Advanced II (400 MHz) spectrometers and MERCURYVX300 using $CDCl_3$ as solvent and tetramethylsilane as the internal standards. High resolution mass spectra (HRMS) were measured by Thermo Scientific LTQ Orbitrap XL mass spectrometer. Thermogravimetric analyses (TGAs) were performed on a NETZSCH STA 449C instrument under nitrogen with a heating rate of 10 ^{o}C min^{-1}. Cyclic voltammetry (CV) was measured on a CHI voltammetric analyzer at room temperature with the conventional three-electrode configuration, consisted of a platinum column working electrode, a platinum wire auxiliary electrode, and an Ag wire pseudo reference electrode. Cyclic voltammograms were recorded using tetrabutylammonium hexafluorophosphate ($TBAPF_6$) (0.1 M) dissolved in solvent (5 mL) as the supporting electrolyte, and ferrocenium-ferrocene (Fc^+/Fc) as the external standard, at the scan rate of 100 mV s^{-1}. The solvent is dichloromethane (DCM) for oxidative scan, and dimethylformamide (DMF) for reductive scan. The onset potential was determined from the intersection of two tangents of the rising and background current in cyclic voltammogram. The geometries and FMOs of ground structure were obtained by B3LYP density functional method with basis set def2-SVP, the excited states of target molecules on optimized ground structure were calculated by PBE0 density functional method with basis set def2-SVP. The ground and excited structure used to calculate RMSD were obtained at def2-SVP/PBE0 level. Relative energy and oscillator strength on dihedral angle θ were obtained at def2-SVP/PBE0 level started from optimized S_1 and S_3 structure with θ increasing or reducing in steps of 2^{o}. θ represents the dihedral angle between the NAI and their linked acridine unit for S_1, and the dihedral angle between the TRZ and their adjacent acridine moiety for S_3. The direction of the calculated transition dipole moment (TDM) was extracted with the nuclear ensemble approach based on the optimized first singlet state geometry according to published work.[2] The spatial range of the volume data were calculated according to the literature method.[3] The isodensity surface of ρ = 0.001 e bohr^{-3} was generated by Marching Tetrahedra (MT) approach with the optimized ground state structure.

Photophysical Characterization

Thin films for photophysical characterization were prepared by thermal evaporation on quartz substrates at 1-2 Å sec^{-1} in a vacuum chamber with a base pressure of $<10^{-6}$. torr. UV-vis absorption spectra were performed on a Shimadzu UV-2700 spectrophotometer. Photoluminescence (PL) spectra, photoluminescence quantum yields (Φ_{PL}s), and phosphorescence spectra were characterized by a spectrofluorimeter (FluoroMax-P, Horiba Jobin Yvon Inc. or F-4600, Hitachi Inc.). Φ_{PL}s of thin films were determined under dry nitrogen environment using these spectrofluorimeters equipped with a calibrated integrating sphere. The transient photoluminescence decay curves were measured by a single photo counting spectrometer from Edinburgh Instruments (FLS920) using a picosecond pulsed UV-LASTER (LASTER377) as the excitation source.

Determination of the Emitting Dipole Orientation of an Emitting Layer

To determine the emitting dipole orientation in a molecular emitting film, angle-resolved and polarization-resolved PL measurements were performed. The sample consisted of a fused silica substrate with the 30-nm-thick mCPCN film doped with the emitter. The sample was attached to a fused silica half cylinder prism by index matching liquid. The excitation of the samples was performed with the 325-nm line of the continuous-wave He:Cd laser with a fixed excitation angle of 45°. The emission angle was changed by the use of an automatic rotation stage. The spectra were resolved by using a *p*-polarizing filter and were measured by a fiber optical spectrometer. The angle-dependent *p*-polarized emission intensity at the peak wavelength of the PL spectrum of the emitting layer was detected. The emitting dipole orientation (the horizontal dipole ratio $\Theta_{//}$) was then determined by least square fitting of the measured angle-dependent *p*-polarized emission intensity with calculated results.

Device Fabrication and Measurement

All organic materials used in experiments (except for the TADF emitters) were purchased from Lumtec, Inc. All compounds were subjected to temperature-gradient sublimation under high vacuum before use. OLEDs were fabricated on the ITO-coated glass substrates with multiple organic layers sandwiched between the transparent bottom indium-tin-oxide (ITO) anode and the top metal cathode. All material layers were deposited by vacuum evaporation in a vacuum chamber with a base pressure of 10^{-6} torr. The deposition system permits the fabrication of the complete device structure in a single vacuum pump-down without breaking vacuum. The deposition rate of organic layers was kept at 0.1 - 0.2 nm s^{-1}. The doping was conducted by co-evaporation from separate evaporation sources with different evaporation rates. The active area of the device is 1 × 1 mm^2, as defined by the shadow mask for cathode deposition. The current density-voltage-brightness (J-V-L) characterization of the light-emitting devices was performed with a source-measurement unit (SMU) and a spectroradiometer (DMS 201, AUTRONIC-MELCHERS GmbH). The EL spectra were measured by a calibrated goniometric spectroradiometer (DMS 201, AUTRONIC-MELCHERS GmbH). The external quantum efficiencies of devices were determined by collecting the total emission fluxes with a calibrated integrating-sphere measurement system and by measuring the angular distribution of the emission spectra and intensities.

Synthetic Routes

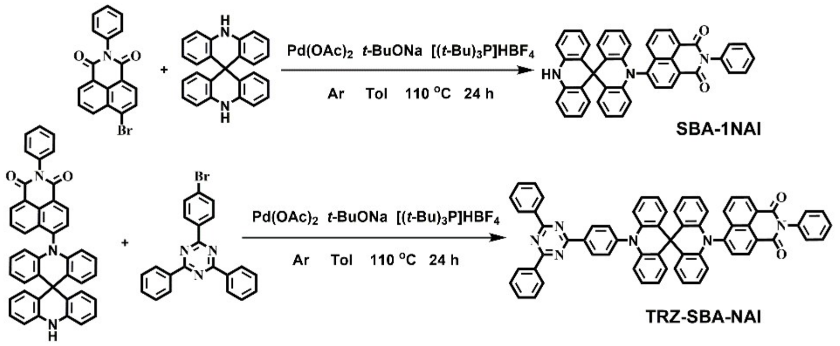

Scheme S1. Synthetic routes of the **TRZ-SBA-NAI**.

*Synthesis of 6-(10H,10'H-9,9'-spirobi[acridin]-10-yl)-2-phenyl-1H-benzo[de]isoquinoline-1,3(2H)-dione (**SBA-1NAI**)*: The SBA-1NAI was synthesized through Buchwald-Hartwig coupling reaction. 9,9'(10*H*,10'*H*)-spirobiacridines (1.73 g, 5.0 mmol), 6-bromo-2-phenyl-1*H*-benzo[*de*]isoquinoline-1,3(2*H*)-dione (1.76 g, 5.0 mmol), sodium *tert*-butoxide (480 mg, 5.0 mmol), palladium(Ⅱ) acetate (34 mg, 0.15 mmol) and tri-*tert*-butylphosphine tetrafluoroborate (131 mg, 0.45 mmol) were dissolved in dry toluene (25 mL) under argon atmosphere. After stirring at 110 °C for 24 hours, the suspension was mixed thoroughly with dichloromethane and washed with water for three times. After drying with anhydrous Na_2SO_4, the organic phase was concentrated and the crude product was purified by column chromatography on silica gel with petroleum ether/dichloromethane (2:3 by vol.) as eluent. Finally, the product was obtained as red powder. 1.27 g, yield: 41%. ^{1}H NMR (400 MHz, $CDCl_3$) δ (ppm): 8.93 (d, *J* = 8 Hz, 1H), 8.75 (d, *J* = 8 Hz, 1H), 8.27 (d, *J* = 8 Hz, 1H), 7.96 (d, *J* = 8 Hz, 1H), 7.79 (t, *J* = 8 Hz, 1H), 7.61 (t, *J* = 8 Hz, 2H), 7.53 (t, *J* = 8 Hz, 1H), 7.39 (d, *J* = 8 Hz, 2H), 7.17-7.11 (m, 5H), 7.07 (t, *J* = 8 Hz, 1H), 6.88-6.72 (m, 8H), 6.37 (s, 1H), 5.98 (d, *J* = 8 Hz, 2H). ^{13}C NMR (100 MHz, $CDCl_3$) δ (ppm): 164.1, 163.8, 144.4, 138.0, 136.4, 135.2, 135.1, 133.2, 133.0, 132.8, 132.5, 132.1, 131.3, 131.2, 131.0, 130.8, 130.7, 130.4, 129.5, 128.9, 128.6, 128.4, 127.3, 127.2, 127.0, 124.0, 123.3, 121.6, 121.1, 120.9, 113.7, 113.5, 113.5, 47.0. HRMS (ESI): *m/z* $[M + H]^+$ calcd for $C_{43}H_{28}N_3O_2^+$: 618.2176; found: 618.2183.

Synthesis of 6-(10'-(4-(4,6-diphenyl-1,3,5-triazin-2-yl)phenyl)-10H,10'H-9,9'-spirobi[acridin]-10-yl)-2-phenyl-1H-benzo[de]isoquinoline-1,3(2H)-dione (***TRZ-SBA-NAI***): SBA-1NAI (1.24 g, 2.0 mmol), 2-(4-bromophenyl)-4,6-diphenyl-1,3,5-triazine (777 mg, 2.0 mmol), sodium *tert*-butoxide (192 mg, 2.0 mmol), palladium(Ⅱ) acetate (14 mg, 0.06 mmol) and tri-*tert*-butylphosphine tetrafluoroborate (52 mg, 0.18 mmol) were dissolved in dry toluene (10 mL) under argon atmosphere. After stirring at 110 °C for 24 hours, the suspension was mixed thoroughly with dichloromethane and washed with water for three times. After drying with anhydrous Na_2SO_4, the organic phase was concentrated and the crude product was purified by column chromatography on silica gel with petroleum ether/dichloromethane (1:3 by vol.) as eluent. Finally, the product was obtained as orange powder. 1.46 g, yield: 79%. ^1H NMR (400 MHz, $CDCl_3$) δ (ppm): 9.13 (d, *J* = 8 Hz, 2H), 8.95 (d, *J* = 8 Hz, 1H), 8.85 (d, *J* = 8 Hz, 4H), 8.77 (d, *J* = 8 Hz, 1H), 8.32 (d, *J* = 8 Hz, 1H), 8.01 (d, *J* = 8 Hz, 1H), 7.82 (t, *J* = 8 Hz, 1H), 7.73 (d, *J* = 8 Hz, 2H), 7.67-7.60 (m, 8H), 7.54 (t, *J* = 8 Hz, 1H), 7.40 (d, *J* = 8 Hz, 2H), 7.33-7.31 (m, 2H), 7,29-7.27 (m, 2H), 7.00 (t, *J* = 8 Hz, 1H), 6.96-6.81 (m, 7H), 6.47 (d, *J* = 8 Hz, 1H), 6.43 (d, *J* = 8 Hz, 1H), 6.06-6.03 (m, 2H). ^{13}C NMR (100 MHz, $CDCl_3$) δ (ppm): 171.9, 171.0, 164.1, 163.7, 145.0, 144.4, 138.9, 137.9, 137.6, 136.5, 136.0, 135.2, 133.2, 133.2, 133.1, 132.8, 132.5, 132.5, 132.0, 131.9, 131.8, 131.7, 131.5, 131.0, 130.8, 130.7, 130.3, 129.5, 129.0, 128.9, 128.8, 128.6, 128.5, 127.0, 127.0, 126.9, 124.0, 123.3, 121.7, 121.3, 121.1, 114.2, 114.1, 113.8, 47.0. HRMS (ESI): *m/z* $[M + H]^+$ calcd for $C_{64}H_{41}N_6O_2^+$: 925.3286; found: 925.3287.

Results and Discussion

structure	HOMO-1	HOMO	LUMO	LUMO+1
S_0 state	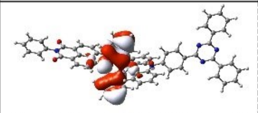	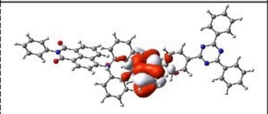	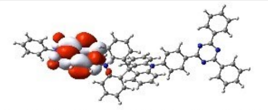	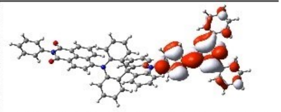
	-5.43 eV	-5.35 eV	-2.76 eV	-2.29 eV
S_1 state	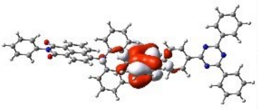	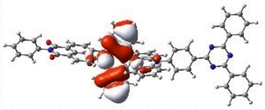	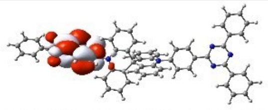	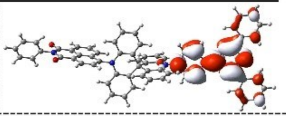
	-5.64 eV	-5.63 eV	-3.00 eV	-2.19 eV

Figure S1. The distribution and energy level of FMOs of **TRA-SBA-NAI** with optimized structure at S_0 state and S_1 state, respectively.

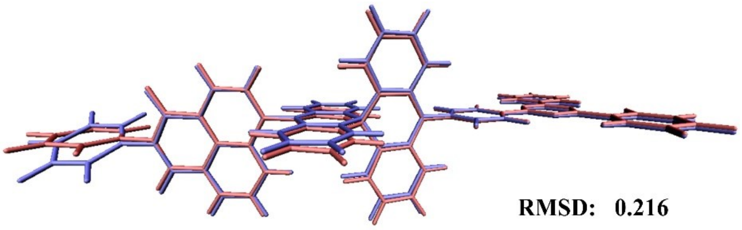

Figure S2. Comparison of optimized structures of **TRZ-SBA-NAI** at S_0 (blue) and S_1 (red) state.

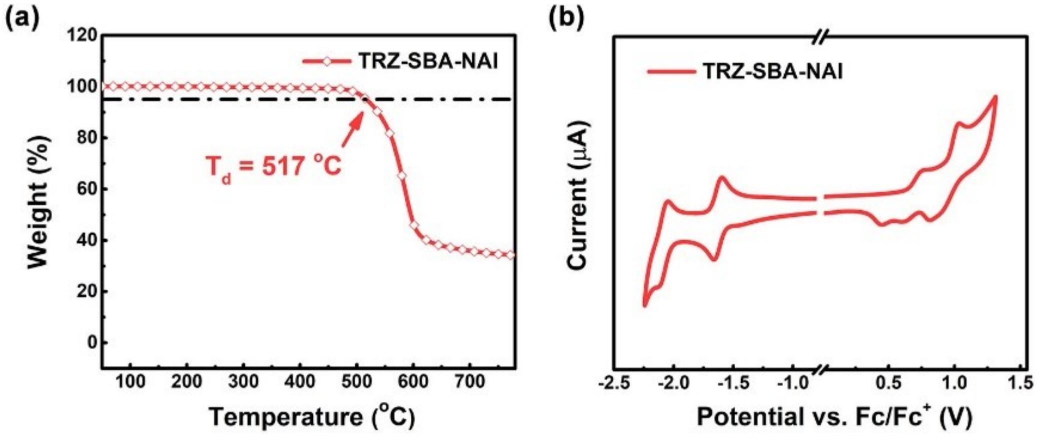

Figure S3. (a) TGA trace of **TRZ-SBA-NAI** recorded at a heating rate of 10 °C min^{-1}. (b) The oxidative scan in DCM and reductive scan in DMF of **TRZ-SBA-NAI**, respectively.

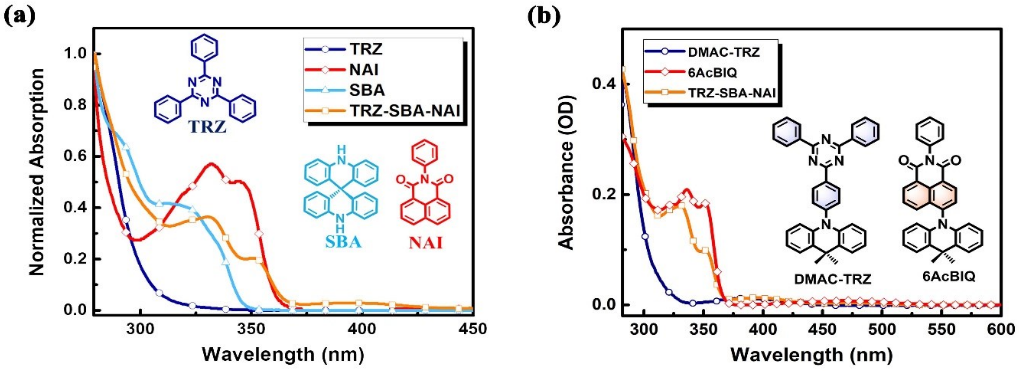

Figure S4. UV-vis absorption spectra of (a) **TRZ-SBA-NAI**, NAI, TRZ, SBA, and (b) **TRZ-SBA-NAI**, **6AcBIQ**, and **DMAC-TRZ** measured in toluene solutions (1 × 10^{-5} M) (Inset: the chemical structures of referred materials).

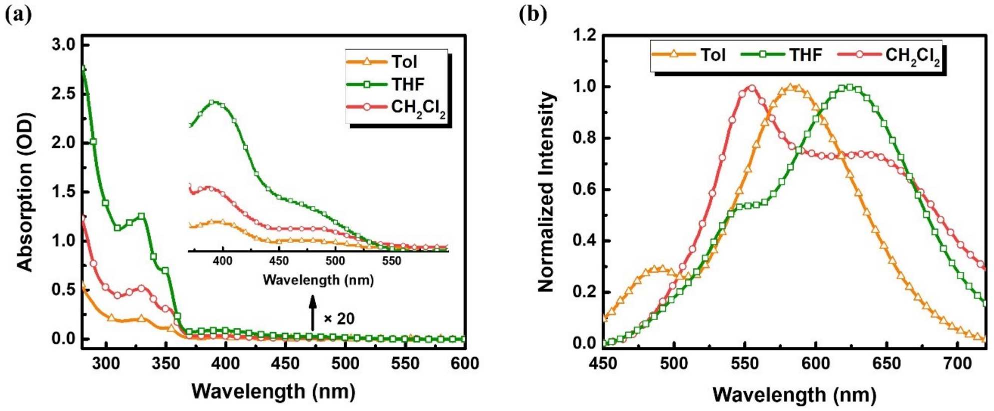

Figure S5. (a) UV-vis absorption spectra and (b) PL spectra of **TRZ-SBA-NAI** measured in toluene, THF, and CH_2CH_2 solutions (1 × 10^{-5} M) at room temperature.

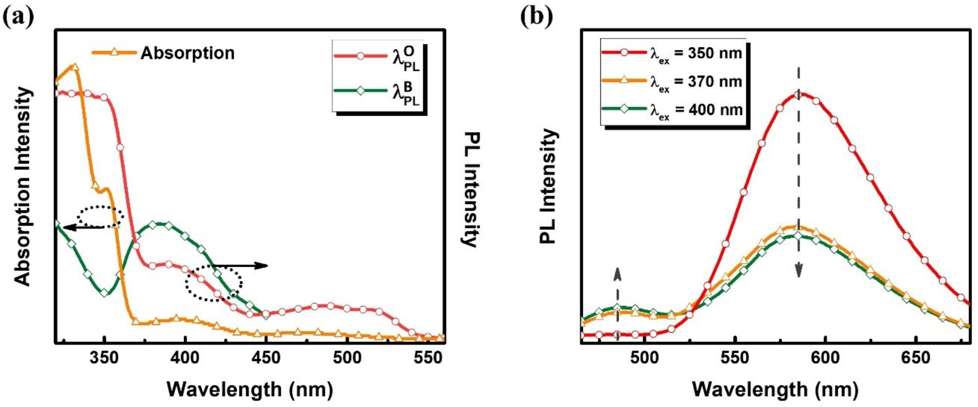

Figure S6. (a) Dependence of the maximum PL intensities of the two emissions of **TRZ-SBA-NAI** at around λ_{PL}^{B} (474 nm) and λ_{PL}^{R} (586 nm) on excitation wavelength in toluene solution (5 × 10^{-5} M). (b) PL spectra of **TRZ-SBA-NAI** measured in toluene solutions (5 × 10^{-5} M) with excitation of 350 nm, 370 nm, and 400 nm, respectively.

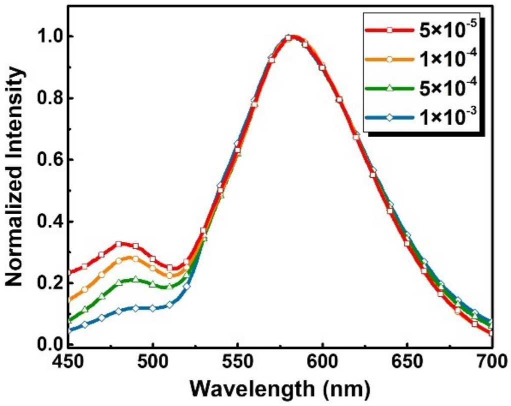

Figure S7. PL spectra of **TRZ-SBA-NAI** measured in toluene with different concentrations at excitation of 370 nm.

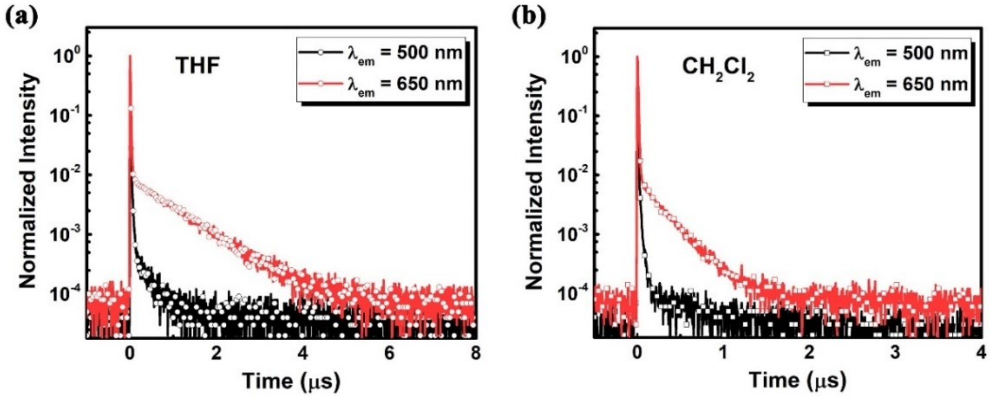

Figure S8. Transient PL spectra of **TRZ-SBA-NAI** measured at different emission in CH_2Cl_2 and THF solution (1 × 10^{-5} M) under degassed conditions.

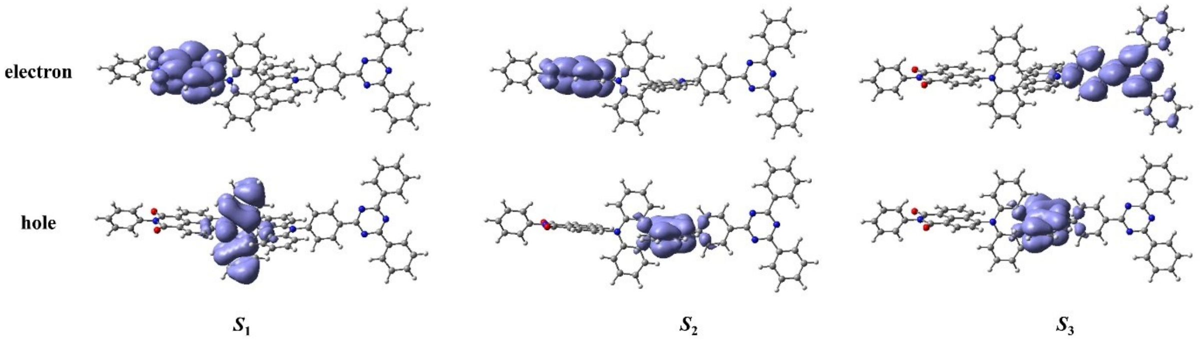

Figure S9. (a) The hole-electron distribution of **TRZ-SBA-NAI** at optimized S_1, S_2, and S_3 states.

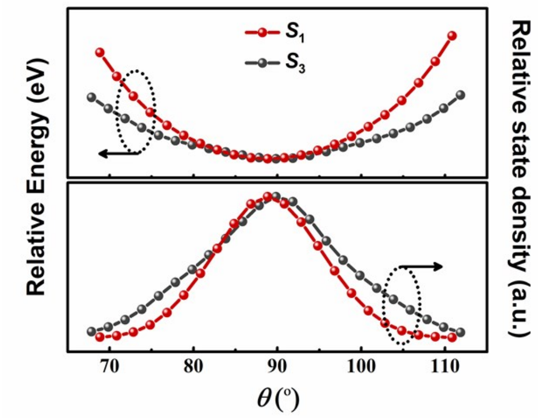

Figure S10. Relative energy and relative state density of S_1 and S_3 on dihedral angle θ between D-A planes.

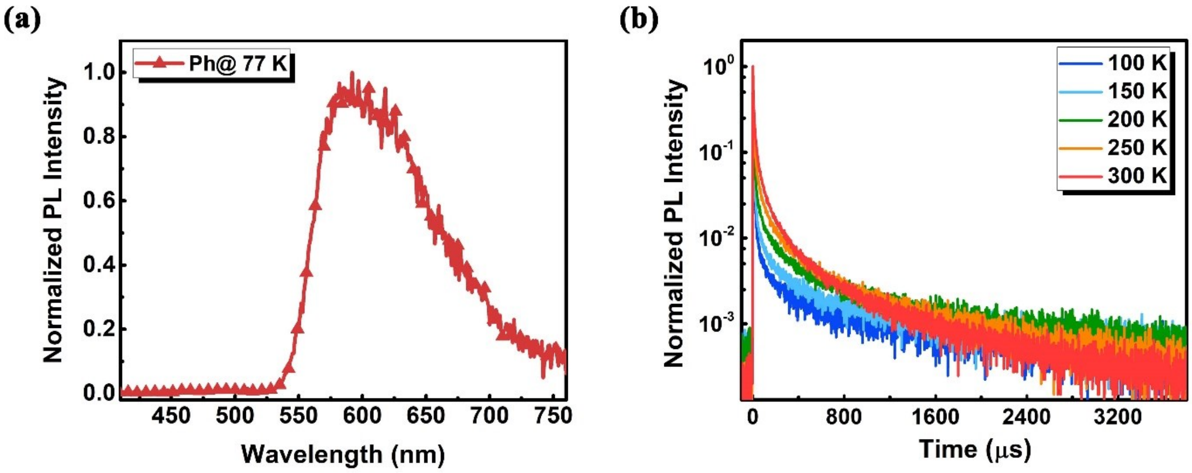

Figure S11. (a) Normalized phosphorescence spectra of 3.0 wt% **TRZ-SBA-NAI** doped into the mCPCN host measured at 77 K. (b) Transient PL spectra of 3.0 wt% **TRZ-SBA-NAI** doped into the mCPCN host measured at temperature varied from 100 K to 300 K under inert condition.

Table S1. The summary of rate constants for **TRZ-SBA-NAI** in the mCPCN host.

Compound	$k_{r,S}$[a] (10^7 s^{-1})	$k_{nr,S}$[b] (10^6 s^{-1})	k_p[c] (10^7 s^{-1})	k_d[d] (10^3 s^{-1})	k_{ISC}[e] (10^7 s^{-1})	k_{RISC}[f] (10^3 s^{-1})	φ_{ISC}[g] (%)
TRZ-SBA-NAI	1.45	2.15	5.98	2.51	4.33	9.10	72

[a]Radiative decay rate of the S_1 state; [b]Nonradiative decay rate of the S_1 state; [c]Decay rate constants for prompt fluorescence; [d]Decay rate constants for delayed fluorescence; [e]Intersystem crossing rate; [f]Reverse intersystem crossing (RISC) rate; [g]Quantum efficiency of intersystem crossing. All above rates were calculated by assuming that most of the triplet states can return to singlet states through RISC and major nonradiative losses occur in singlet states.[4]

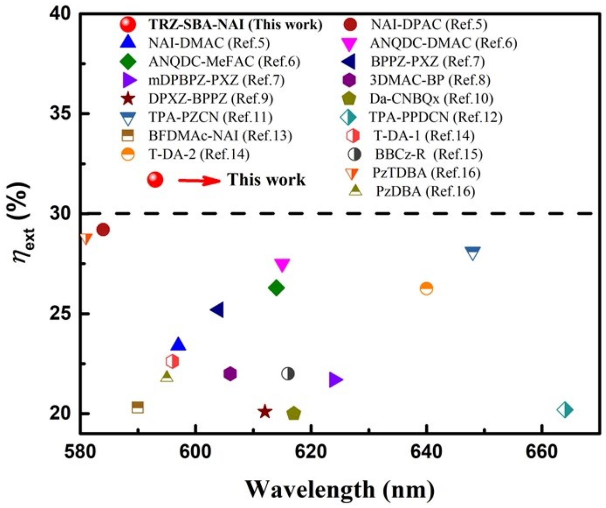

Figure S12. η_{ext} versus EL peak wavelength of the representative orange-red OLEDs based on TADF emitters with EL_{peak} ≥ 580 nm and η_{ext} ≥ 20% reported in the literature.[5-16]

Table S2. The characteristics of the representative orange-red OLEDs based on TADF emitters with EL_{peak} ≥ 580 nm and η_{ext} ≥ 20%. Device data are taken from the previous literature.[5-16]

Emitter	η_{ext} (%)	η_p (lm W^{-1})	η_c (cd A^{-1})	V_{on} (V)	EL_{peak} (nm)	CIE (x, y)	Ref.
TRZ-SBA-NAI	**31.7**	**79.6**	**71.0**	**2.9**	**593**	**0.55, 0.45**	**This work**
NAI-DPAC	29.2	79.7	76.2	3.0	584	0.52, 0.47	5
NAI-DMAC	23.4	53.1	50.7	3.0	597	0.56, 0.44	5
ANQDC-DMAC	27.5	53.1	47.6	2.7	615	0.58, 0.41	6
ANQDC-MeFAC	26.3	46.5	41.4	2.9	614	0.60, 0.40	6
BPPZ-PXZ	25.2	41	37	-	604	0.57, 0.43	7
mDPBPZ-PXZ	21.7	21	25	-	624	0.62, 0.38	7
3DMAC-BP	22	36.4	38.2	3.1	606	0.58, 0.41	8
DPXZ-BPPZ	20.1	30.9	30.2	3.1	612	0.60, 0.40	9
Da-CNBQx	20	-	-	2.8	617	0.59, 0.41	10
TPA-PZCN	28.1	26.3	20.0	2.4	648	0.66, 0.34	11
TPA-PPDCN	20.2	8.8	8.4	3.2	664	0.68, 0.32	12
BFDMAc-NAI	20.3	51.4	49.2	3.0	590	-	13
T-DA-1	22.62	53.58	51.17	3.0	596	0.54, 0.46	14
T-DA-2	26.26	22.48	24.44	3.0	640	0.62, 0.37	14
BBCz-R	22.0	-	-	-	616	0.67, 0.33	15
PzTDBA	28.8	-	60.6	2.7	581	0.51, 0.48	16
PzDBA	21.8	-	35.7	2.7	595	0.55, 0.45	16

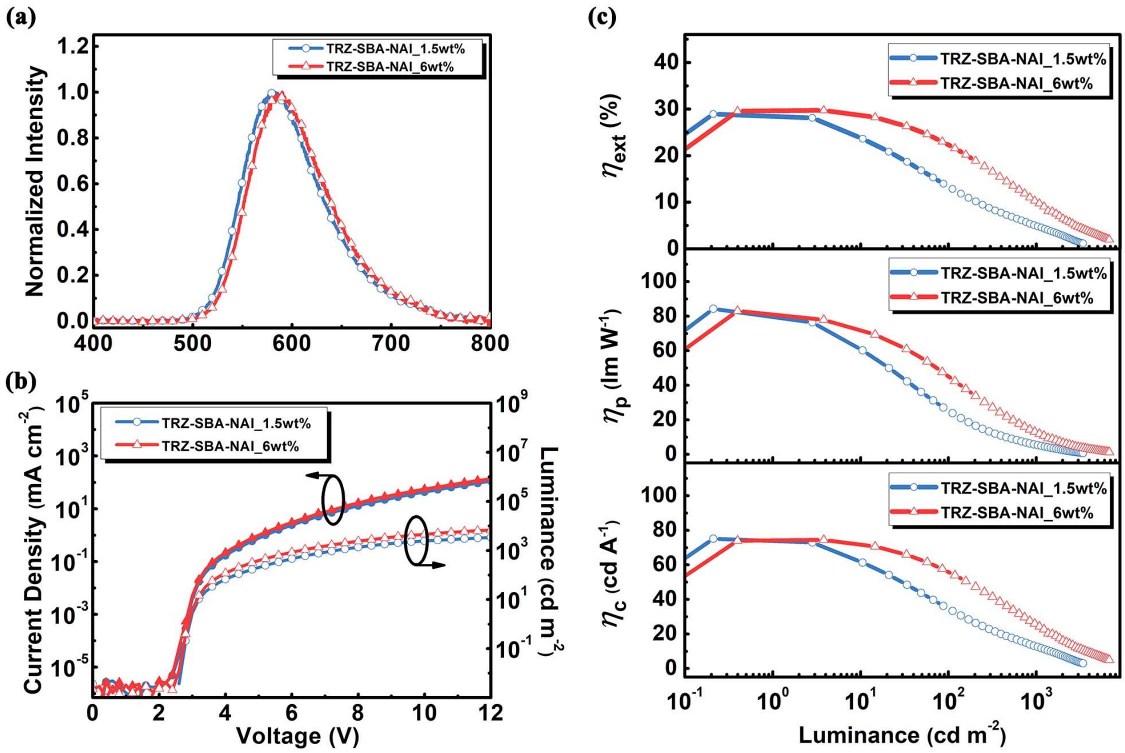

Figure S13. (a) Electroluminescent spectra, (b) current density-voltage-luminance characteristics and (c) external quantum efficiency, power efficiency and current efficiency versus luminance curves of the devices. Device structure: ITO/MoO$_3$ (2 nm)/TAPC (60 nm)/mCP (10 nm)/mCPCN: *x* wt% **TRZ-SBA-NAI** (20 nm)/3TPYMB (60 nm)/LiF (1 nm)/Al.

Table S3. The key electroluminescent data of **TRZ-SBA-NAI**-based device.

Device	V_{on}[a] (V)	EL_{peak}[b] (nm)	η_{ext}[c] (%)	η_p[d] (lm W^{-1})	η_c[e] (cd A^{-1})	Roll-Off[f] (%)	CIE(x,y)
TRZ-SBA-NAI_1.5wt%	2.9	585	28.9, 13.4, 4.9	75.1, 34.8, 12.8	84.3, 25.5, 5.5	53.6, 83.0	0.53,0.47
TRZ-SBA-NAI_3 wt%	2.9	593	31.7, 16.5, 6.4	79.6, 24.1, 5.6	71.0, 36.3, 14.2	47.9, 79.8	0.55,0.45
TRZ-SBA-NAI_6 wt%	2.9	590	29.7, 22.4, 10.3	83.0, 45.3, 12.9	74.4, 55.9, 25.6	24.6, 65.3	0.54,0.46

[a] The turn-on voltage recorded at a brightness of 1 cd m^{-2}; [b] Emission peak of electroluminescent spectra; Maximum value, values at 100 and 1000 cd m^{-2} of [c] external quantum efficiency, [d] power efficiency and [e] current efficiency; [f] external quantum efficiency roll-offs at 100 and 1000 cd m^{-2}.

NMR and HRMS Spectra

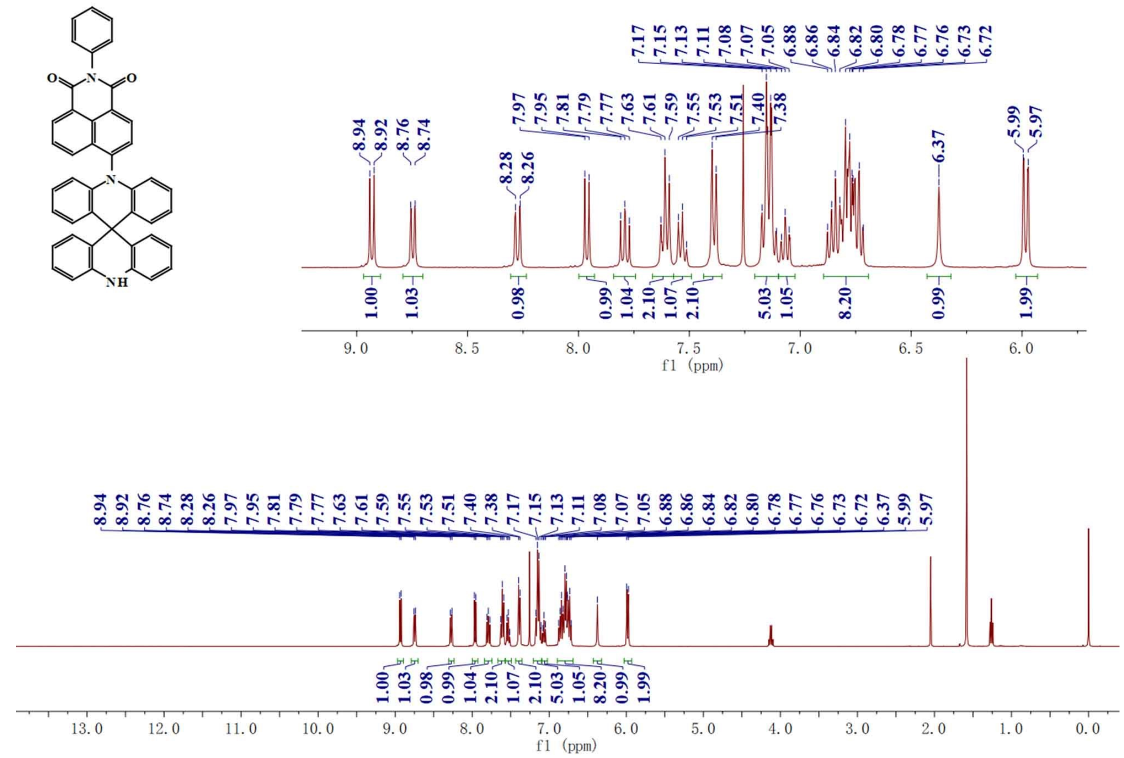

Figure S14. ^{1}H NMR spectra of SBA-1NAI (400 MHz, $CDCl_3$ + TMS, 25 ^{o}C).

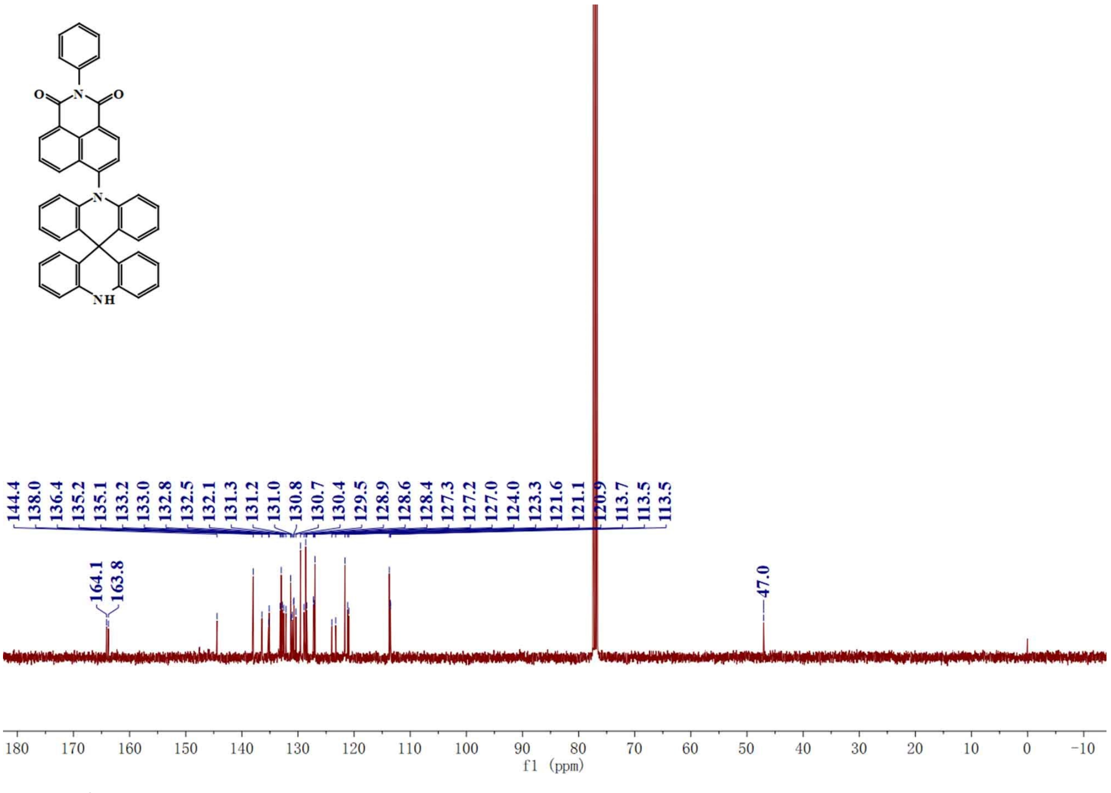

Figure S15. ^{13}C NMR spectra of SBA-1NAI (100 MHz, $CDCl_3$ + TMS, 25 ^{o}C).

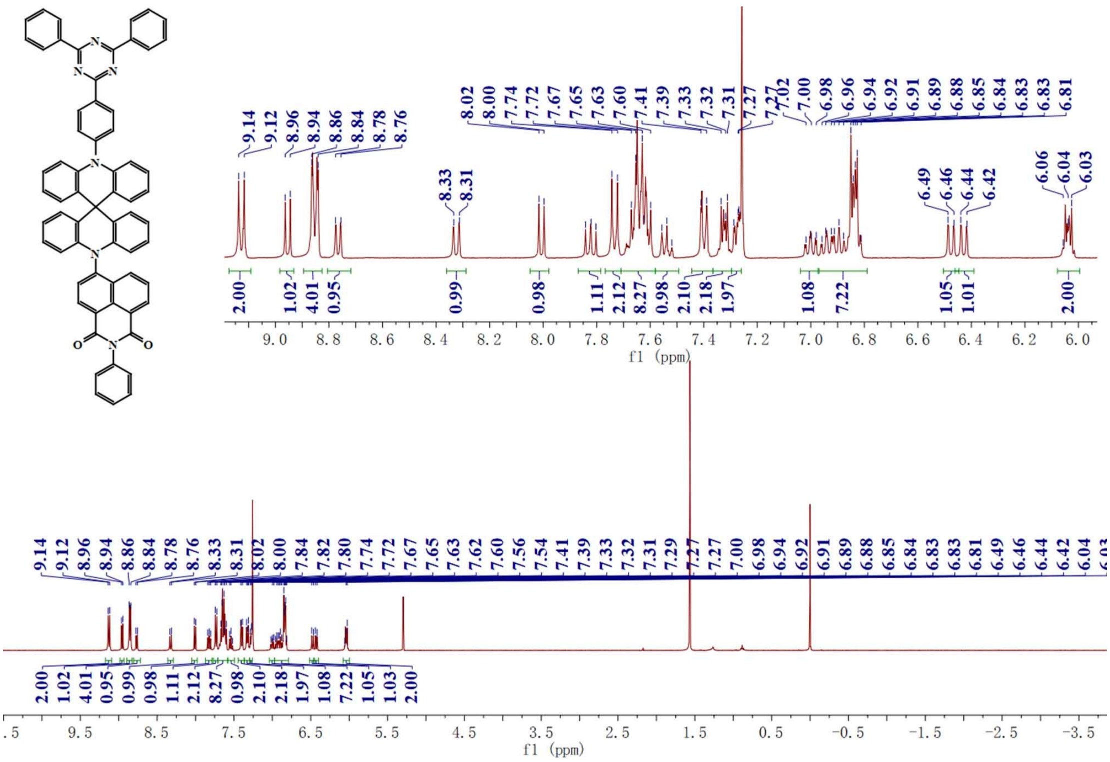

Figure S16. ^{1}H NMR spectra of **TRZ-SBA-NAI** (400 MHz, $CDCl_3$ + TMS, 25 ^{o}C).

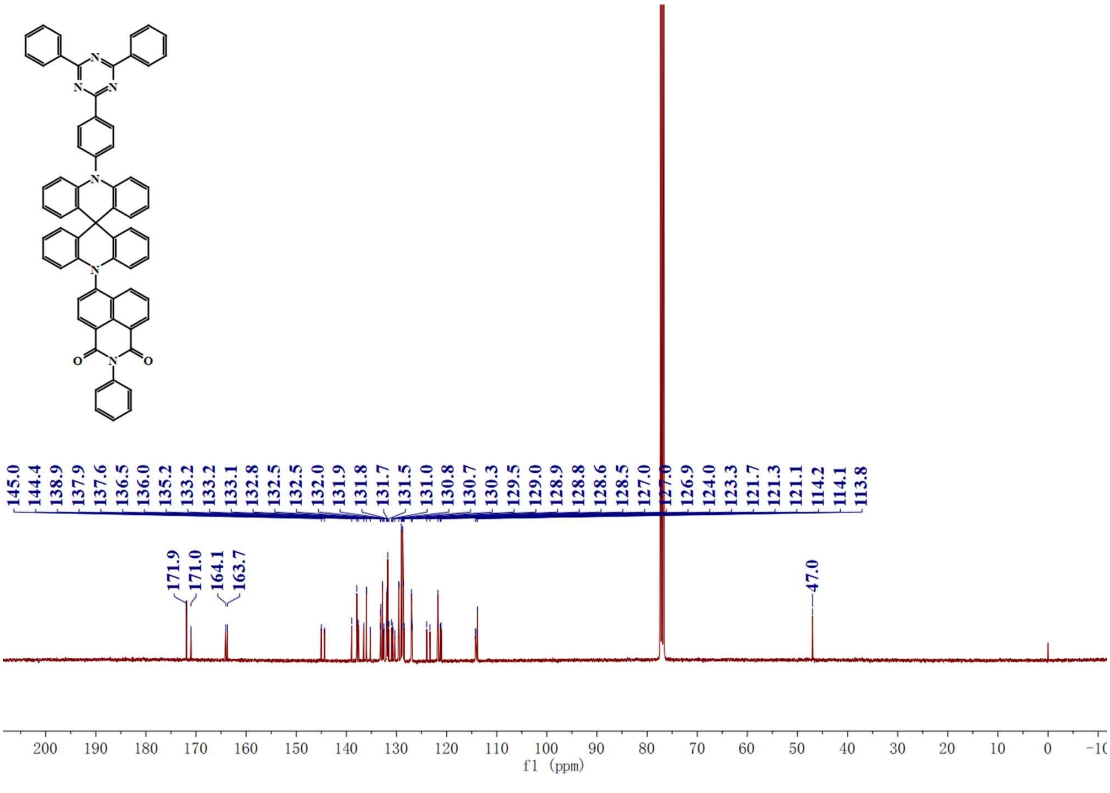

Figure S17. ^{13}C NMR spectra of **TRZ-SBA-NAI** (100 MHz, $CDCl_3$ + TMS, 25 ^{o}C).

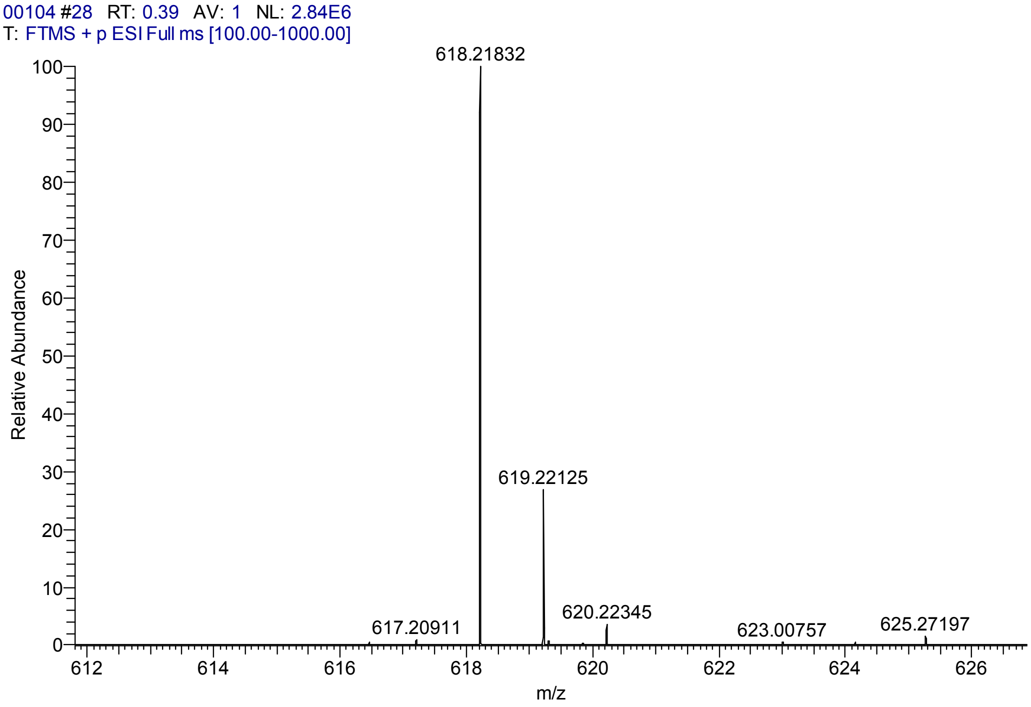

Figure S18. HRMS spectra of **SBA-1NAI**.

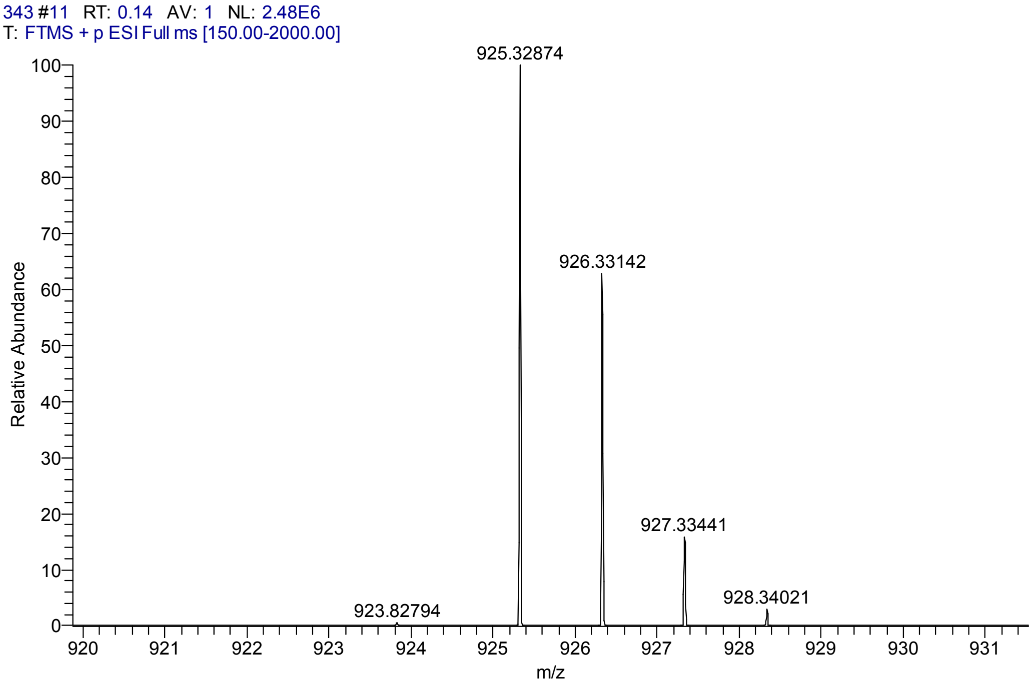

Figure S19. HRMS spectra of **TRZ-SBA-NAI**.

References

1 W.-L. Tsai, M.-H. Huang, W.-K. Lee, Y.-J. Hsu, K.-C. Pan, Y.-H. Huang, H.-C. Ting, M. Sarma, Y.-Y. Ho, H.-C. Hu, C.-C. Chen, M.-T. Lee, K.-T. Wong and C.-C. Wu, *Chem. Commun.*, 2015, **51**, 13662-13665.

2 W. Zeng, S. Gong, C. Zhong and C. Yang, *J. Phys. Chem. C*, 2019, **123**, 10081-10086.

3 T. Lu and F. Chen, *J. Mol. Graphics Modell.*, 2012, **38**, 314-323.

4 K.-C. Pan, S.-W. Li, Y.-Y. Ho, Y.-J. Shiu, W.-L. Tsai, M. Jiao, W.-K. Lee, C.-C. Wu, C.-L. Chung, T. Chatterjee, Y.-S. Li, K.-T. Wong, H.-C. Hu, C.-C. Chen and M.-T. Lee, *Adv. Funct. Mater.*, 2016, **26**, 7560-7571.

5 W. Zeng, H.-Y. Lai, W.-K. Lee, M. Jiao, Y.-J. Shiu, C. Zhong, S. Gong, T. Zhou, G. Xie, M. Sarma, K.-T. Wong, C.-C. Wu and C. Yang, *Adv. Mater.*, 2018, **30**, 1704961.

6 X. Gong, P. Li, Y.-H. Huang, C.-Y. Wang, C.-H. Lu, W.-K. Lee, C. Zhong, Z. Chen, W. Ning, C.-C. Wu, S. Gong and C. Yang, *Adv. Funct. Mater.*, 2020, **30**, 1908839.

7 J.-X. Chen, W.-W. Tao, W.-C. Chen, Y.-F. Xiao, K. Wang, C. Cao, J. Yu, S. Li, F.-X. Geng, C. Adachi, C.-S. Lee and X.-H. Zhang, *Angew. Chem. Int. Ed.*, 2019, **58**, 14660-14665.

8 F.-M. Xie, H.-Z. Li, G.-L. Dai, Y.-Q. Li, T. Cheng, M. Xie, J.-X. Tang and X. Zhao, *ACS Appl. Mater. Interfaces*, 2019, **11**, 26144-26151.

9 J.-X. Chen, K. Wang, C.-J. Zheng, M. Zhang, Y.-Z. Shi, S.-T. Tao, H. Lin, W. Liu, W.-W. Tao, X.-M. Ou and X.-H. Zhang, *Adv. Sci.*, 2018, **5**, 1800436.

10 R. Furue, K. Matsuo, Y. Ashikari, H. Ooka, N. Amanokura and T. Yasuda, *Adv. Opt. Mater.*, 2018, **6**, 1701147.

11 Y.-L. Zhang, Q. Ran, Q. Wang, Y. Liu, C. Hanisch, S. Reineke, J. Fan and L.-S. Liao, *Adv. Mater.*, 2019, **31**, 1902368.

12 T. Yang, B. Liang, Z. Cheng, C. Li, G. Lu and Y, Wang, *J. Phys. Chem. C*, 2019, **123**, 18585-18592.

13 T. Chen, C.-H. Lu, C.-W. Huang, X. Zeng, J. Gao, Z. Chen, Y. Xiang, W. Zeng, Z. Huang, S. Gong, C.-C. Wu and C. Yang, *J. Mater. Chem. C*, 2019, **7**, 9087-9094.

14 T. Yang, Z. Cheng, Z. Li, J. Liang, Y. Xu, C. Li and Y. Wang, *Adv. Funct. Mater.*, 2020, **30**, 2002681.

15 M. Yang, I. S. Park and T. Yasuda, *J. Am. Chem. Soc.*, 2020, **142**, 19468-19472.

16 D. Karthik, Y. H. Jung, H. Lee, S. Hwang, B.-M. Seo, J.-Y. Kim, C. W. Han and J. H. Kwon, *Adv. Mater.*, 2021, **33**, 2007724.